PET/MRI of Hypoxic Atherosclerosis Using ^{64}Cu-ATSM in a Rabbit Model

Xingyu Nie[1,2], Richard Laforest[1], Andrew Elvington[3], Gwendalyn J. Randolph[3], Jie Zheng[1], Tom Voller[1], Dana R. Abendschein[3,4], Suzanne E. Lapi[1–3], and Pamela K. Woodard[1,2,5]

[1]Mallinckrodt Institute of Radiology, Washington University School of Medicine, St. Louis, Missouri; [2]Department of Biomedical Engineering, Washington University in St. Louis, St. Louis, Missouri; [3]Division of Biology and Biomedical Sciences, Washington University in St. Louis, St. Louis, Missouri; [4]Center for Cardiovascular Research, Department of Internal Medicine, Washington University School of Medicine, St. Louis, Missouri; and [5]Diabetic Cardiovascular Disease Center, Washington University in St. Louis, St. Louis, Missouri

The macrophage-rich core of advanced human atheroma has been demonstrated to be hypoxic, which may have implications in plaque stability. The goal of this study was to determine the feasibility of the hypoxia PET imaging agent ^{64}Cu-ATSM to detect hypoxia in a rabbit model of atherosclerosis imaged on a simultaneous PET/MR scanner, using MR for both attenuation correction and depiction of lesion location. **Methods:** New Zealand White rabbits fed a Western diet for 4–6 wk underwent endothelial denudation of the right femoral artery by air desiccation to induce an atherosclerotic-like lesion and underwent a sham operation on the left femoral artery. Four and 8 wk after injury, a 0- to 60-min dynamic whole-body PET/MR examination was performed after injection of approximately 111 MBq of ^{64}Cu-ATSM. After 24 h, a 0- to 75-min dynamic PET/MR examination after injection of approximately 111 MBq of ^{18}F-FDG was performed. The rabbits were euthanized, and the injured femoral artery (IF) and sham-operated femoral artery (SF) were collected for immunohistochemistry assessment of hypoxic macrophages (hypoxia marker pimonidazole, macrophage marker RAM-11, and hypoxia-inducible factor-1 α subunit [HIF-1α]). Regions of interest of IF, SF, and background muscle (BM) were drawn on fused PET/MR images, and IF-to-BM and SF-to-BM SUV ratios were compared using the Student *t* test. **Results:** Elevated uptake of ^{64}Cu-ATSM was found in the rabbits' IF compared with the SF. ^{64}Cu-ATSM imaging demonstrated IF-to-SF SUV_{mean} ratios (±SD) of 1.75 ± 0.21 and 2.30 ± 0.26 at 4 and 8 wk after injury, respectively. ^{18}F-FDG imaging demonstrated IF-to-SF SUV_{mean} ratios of 1.84 ± 0.12 at 8 wk after injury. IF-to-BM SUV_{mean} ratios were significantly higher ($P < 0.001$) than SF-to-BM SUV_{mean} ratios both 4 and 8 wk after injury for ^{64}Cu-ATSM and 8 wk after injury for ^{18}F-FDG ($P < 0.05$). Pimonidazole immunohistochemistry at 8 wk colocalized to RAM-11 and HIF-1α. **Conclusion:** The results show that hypoxia is present in this rabbit model of atherosclerosis and suggest that ^{64}Cu-ATSM PET/MR is a potentially promising method for the detection of hypoxic and potentially vulnerable atherosclerotic plaque in human subjects.

Key Words: ^{64}Cu-ATSM; PET/MR; hypoxic atherosclerosis; rabbit model

J Nucl Med 2016; 57:2006–2011
DOI: 10.2967/jnumed.116.172544

Atherosclerosis is a systemic degenerative and inflammatory vascular disease that develops over decades, leading to advanced lesions characterized by a lipid core separated from the lumen by a fibrous cap. It has been recognized that plaque composition more than the degree of luminal stenosis determines the risk of acute clinical events (e.g., stroke, myocardial infarction) (*1*). Macrophage-rich plaques with a thin fibrous cap, large lipid core, and abundance of leaky microvessels tend to be more vulnerable (*1*). The rupture or erosion of the fibrous cap in vulnerable plaque may lead to thromboembolization and arterial occlusion (*2,3*).

According to the anoxemia theory of atherosclerosis, an imbalance between the demand for and supply of oxygen in the arterial wall is a key factor in the development of atherosclerotic lesions (*4*). In the initial stages of atherogenesis, modified lipoproteins recruit monocytes and T cells. Macrophages internalize the modified lipoproteins, resulting in the accumulation of high-oxygen-consuming, high-metabolic-rate, lipid-loaded macrophages (foam cells) in developing lesions (*5,6*). The combination of increased oxygen demand together with impaired oxygen diffusion capacity results in the presence of severe hypoxia (<1% oxygen) in macrophage-rich zones (150–300 μm) into the lesion (*7–9*). There is growing evidence that zones of hypoxia occur at depth in the atherosclerotic plaque (*6,8*). Leppanen et al. (*6*) suggested that over time macrophages within the plaque core become adenosine triphosphate–depleted and severely hypoxic, contributing to their death and formation of a necrotic core that increases angiogenesis and plaque destabilization. Sluimer et al. (*9*) demonstrated the direct presence of hypoxia in the macrophage-rich regions of advanced human carotid atherosclerotic plaques using the hypoxia marker pimonidazole, correlating hypoxia with CD68-positive macrophages, and angiogenesis.

Our study investigated the hypoxia PET imaging agent ^{64}Cu-ATSM in a PET/MR hybrid scanner for detecting hypoxic atherosclerosis in an animal model. The PET/MR imaging strategy uses MRI for attenuation correction and for colocalization of ^{64}Cu-ATSM uptake on PET to the rabbit femoral artery lesion depicted anatomically on a 3-T MR image. ^{64}Cu-ATSM is of particular interest because advanced atheromas in human carotids leading to angiogenesis and thrombosis (i.e., unstable or vulnerable plaques) have been shown to be hypoxic (*9*). Thus, this hypoxic cell–avid PET agent, which is already in use in human patients for imaging tumor hypoxia, has the potential to translate into human subjects for atherosclerosis imaging. In this paper, we show that ^{64}Cu-ATSM can detect hypoxia in an

Received Jan. 20, 2016; revision accepted Jun. 7, 2016.
For correspondence or reprints contact: Pamela K. Woodard, 510 South Kingshighway Blvd. #8223, St. Louis, MO 63110-1076.
E-mail: woodardp@mir.wustl.edu
Published online Jul. 7, 2016.

animal model with atherosclerotic-like lesions and that hypoxia in these lesions as determined by ^{64}Cu-ATSM uptake on PET and pimonidazole staining of the ex vivo specimen obtained after imaging colocalizes to macrophages.

MATERIALS AND METHODS

General

Animal studies were performed under a protocol approved by the Animal Studies Committee at our institution. Advanced atherosclerotic-like lesions were induced in the right femoral arteries of 5 New Zealand White rabbits weighing 2.5–3 kg by endothelial denudation with air desiccation 2–4 wk after the start of a Western diet (0.25% cholesterol; Purina TestDiet) (*10,11*), depending on when the serum cholesterol level of the rabbits exceeded 2 mg/mL. The left femoral artery underwent a sham operation as the negative control. At the end of the last imaging procedure, the anesthetized animals were euthanized by exsanguination and the arterial segments collected for immunohistochemistry.

All chemicals, unless otherwise stated, were purchased from Sigma-Aldrich Chemical Co. Water was distilled and then deionized (18 MΩ/cm^2) by being passed through a Milli-Q water filtration system (Millipore Corp.). ^{64}Cu was prepared as previously described (*12*). Radioactivity was counted with a Beckman γ-8000 counter containing a NaI crystal (Beckman Instruments, Inc.). EM Science Silica Gel 60 F254 thin-layer chromatography plates (10 × 5 cm) were purchased from EMD Millipore Corp. Radioactive thin-layer chromatography plates were analyzed using a Bioscan System 200 plate reader (Bioscan, Inc.).

Diacetyl-bis (N^4-methylthiosemicarbazonate) (H_2-ATSM) was labeled with ^{64}Cu as per our standard methods (*13*). Briefly, 1 mg of ASTM powder was dissolved in 1 mL of dimethyl sulfoxide to give an overall concentration of 1 mg/mL. A total of 10 μL (10 μg) of this solution was then added to 4 μL (~370 MBq) of $^{64}CuCl_2$ in 200 μL of 1 M NaOAc or 3 M HCl buffer. This solution was then stirred for 3–5 min and allowed to sit briefly at room temperature, after which it was loaded onto a C_{18} Sep-Pak Light (Waters Corp.), which had been preconditioned with 5 mL of ethanol and 5 mL of water. After the sample was loaded, 10 mL of water were passed through to remove the dimethyl sulfoxide and any unreacted ^{64}Cu. The labeled complex was then eluted in 350 μL of ethanol (after a 150-μL ethanol elution for the void volume), from which approximately 111 MBq (3 mCi) of the compound were extracted and diluted into 3 mL of saline before injection. The purity of the labeled material was determined by radioactive thin-layer chromatography plates using silica gel plates with ethyl acetate as the mobile phase. Radiochemical yield was 80%–85% and purity greater than 95%.

Imaging Protocol

The rabbits underwent simultaneous PET/MR (Siemens Biograph mMR) examination 4 and 8 wk after arterial injury operation (Fig. 1). At each time point, a 0- to 60-min dynamic whole-body PET/MR examination was performed after injection of approximately 111 MBq of ^{64}Cu-ATSM. At the second time point, an additional 0- to 75-min dynamic PET/MR examination after injection of approximately 111 MBq of ^{18}F-FDG was performed.

During PET acquisition, MR scans consisting of T1-weighted 2-dimensional (2D) turbo-spin echo (TSE) (repetition time [TR]/echo time [TE], 600/11 ms; number of slices, 16; field of view, 60 × 120 mm; matrix size, 384 × 768), T2-weighted 2D TSE (TR/TE, 2,200–2,890/56 ms; number of slices, 16; field of view, 60 × 120 mm; matrix size, 384 × 768), and proton density (PD)–weighted 2D TSE (TR/TE, 2,200–2,890/11 ms; number of slices, 16; field of view, 60 × 120 mm; matrix size, 384 × 768) were obtained. The following were parameters for all sequences: magnetic field strength, 3T; pixel bandwidth, 260 kHz; flip angle, 124°–151°; echo train length, 7; in-plane resolution, 0.16 × 0.16 mm; slice thickness, 2 mm; and signal averages, 10–12.

The data from the last 30 min of each PET scan were used for high-definition PET imaging reconstruction, performed on the Siemens e7-tools software using a point spread function–corrected ordinary Poisson ordered-subsets expectation maximization algorithm with 21 subsets, 8 iterations, and a gaussian smoothing filter of 2 mm in full width at half maximum. The size of the image matrices was 344 × 344 × 127, resulting in a pixel size of 1.04 mm and a slice thickness of 2.03 mm. MR-based 2-point Dixon attenuation correction for the PET image was also performed. Dynamic images were decay-corrected to the injection time. An average PET spatial resolution of 4.3 mm at 1 cm offset from the center of the field of view was expected to be obtained from the PET/MR scanner (*14*).

Image Analysis

PET images were coregistered with MR images using Inveon Research Workplace (Siemens Medical Solutions USA, Inc.) to identify the location of the plaques developed in the femoral artery. The fused images were evaluated by measuring the radioactivity concentration within the regions of interest drawn on the injured femoral artery and sham-operated femoral artery and a representative area on the nontarget background thigh muscle of each rabbit.

The SUV_{mean} and SUV_{max} of IF, SF, and BM were calculated by dividing the decay-corrected activity per unit volume of tissue (Bq/cm^3) by the injected activity per unit of body weight (Bq/g), as described by the following equation:

$$\mathrm{SUV} = \frac{\text{radioactivity concentration (Bq/cm}^3\text{)}}{\text{injected dose (Bq)/body weight (g)}}$$

The mean cross-sectional area of the femoral artery blood vessel wall was measured in transverse MR images by subtracting the number of pixels of the inner blood vessel from the outside blood vessels in transverse MR images and taking the average of the slices containing the plaque.

Histologic Analysis

The animals were injected intravenously with the hypoxia-reactive reagent pimonidazole hydrochloride (Hypoxyprobe-1; Natural Pharmacia International) 1.5–2 h before euthanasia. The IF and SF were collected and perfusion-fixed with freshly prepared 3%–4% paraformaldehyde solution to collect specimens for histopathologic assessment. Specimens were embedded in paraffin and sectioned transversely. To visualize the spatial colocalization of the hypoxic cells and macrophages, adjacent 5-μm-thick cross-sections of the femoral artery were obtained.

IF and SF specimens were stained for the presence of hypoxia using the antipimonidazole antibody (Natural Pharmacia Inc.) and mounted in solution containing 4′-6-diamidino-2-phenylindole (DAPI; Vector Laboratories) for fluorescent staining of nuclei. Although pimonidazole may react with reactive oxygen species, the antipimonidazole antibody recognizes only hypoxia derivatives (*9*). Fluorescein isothiocyanate was used as the secondary antibody.

Adjacent serial sections were assessed for macrophage content and hypoxia-inducible factor-1α (HIF-1α) using mouse monoclonal antibodies for rabbit macrophages (clone RAM-11; Dako North America, Inc.) and anti-HIF-1α (clone H1α67; Novus Biologicals).

The bound markers were detected by Cy3 and Cy2 secondary fluorescent antibodies, respectively. The slides were incubated with DAPI before cover-slipping. Negative control staining was performed

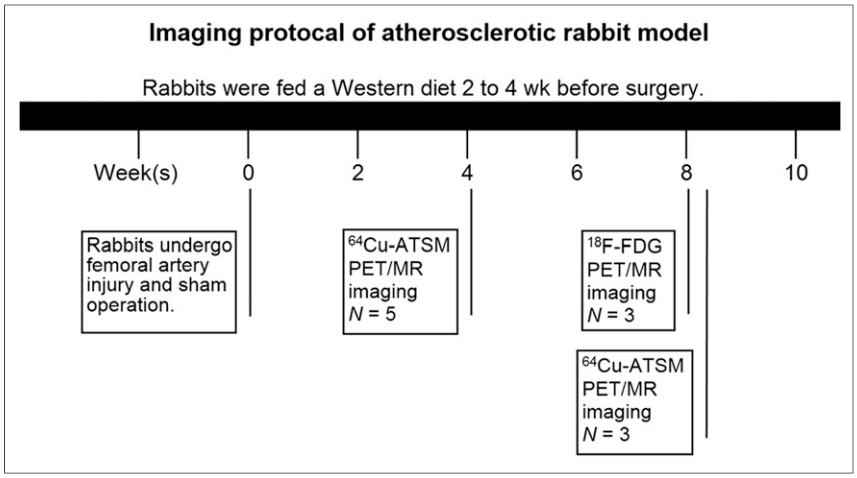

FIGURE 1. Study protocol for imaging atherosclerotic rabbits.

by replacing the primary antibody with a matching isotype control followed by the same fluorescent-labeled secondary antibody. Immunohistochemistry slides were imaged using a Leica TCS SP5 confocal laser scanning microscope.

Statistical Methods

Data are presented as mean ± SD. Statistical analysis was performed using GraphPad Prism 6 (GraphPad Software, Inc.). Differences between the IF-to-BM and SF-to-BM SUV were assessed using the Student *t* test. The correlation between the IF-to-SF femoral artery cross-section area ratios in MR images and the IF-to-SF SUV ratios in the corresponding ^{64}Cu-ATSM PET images were analyzed by simple linear regression with 95% confidence intervals. A *P* value of less than 0.05 was considered statistically significant.

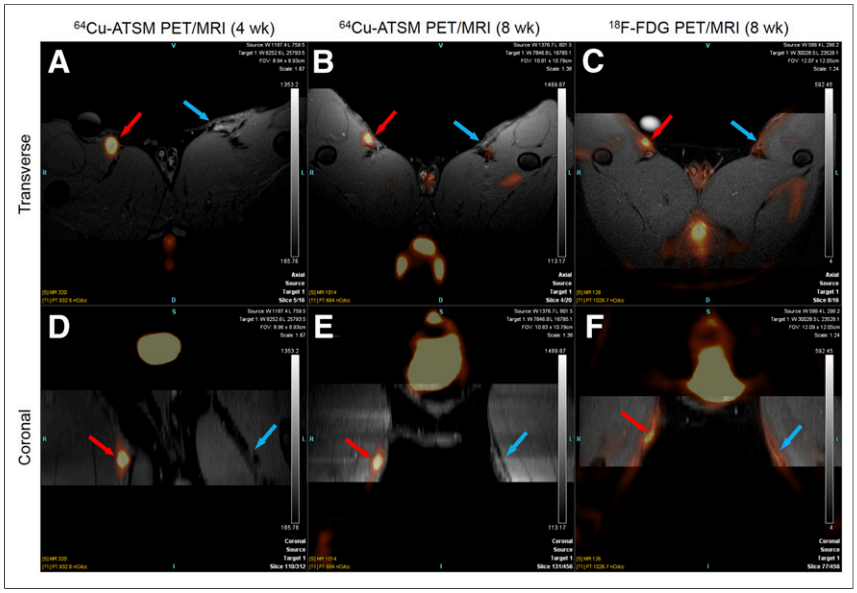

FIGURE 2. Transverse (top) and coronal (bottom) view of ^{64}Cu-ATSM PET/T1-weighted MR images of representative rabbit at 4 wk (A, D) and 8 wk (B, E) after injury and ^{18}F-FDG PET/T1-weighted MR images of same rabbit 8 wk after injury (C, F). Red arrows point to injured femoral artery; blue arrows point to sham-operated femoral artery.

RESULTS

PET/MR imaging showed increased uptake of ^{64}Cu-ATSM in the IF of all 5 rabbits 4 wk after injury, as indicated by the bright spots in both transverse and coronal views colocalizing to the lesion as identified by anatomic MRI (Figs. 2A and 2D; Supplemental Fig. 1 [supplemental materials are available at http://jnm.snmjournals.org]). Eight weeks after injury, significantly higher ^{64}Cu-ATSM was found in IF in the PET images fused with T1-weighted MRI, T2-weighted MRI, and PD-weighted MRI (Figs. 2B and 2E; Supplemental Fig. 2, PD-weighted MRI not shown). Higher uptake of ^{18}F-FDG in the IF of the rabbits confirmed the development of advanced atherosclerotic-like plaque (Figs. 2C and 2F; Supplemental Fig. 3).

The IF demonstrated 1.75 ± 0.21- and 2.30 ± 0.26-fold-higher SUV_{mean} ratios and 1.61 ± 0.15- and 1.84 ± 0.12-fold-higher SUV_{max} ratios 30–60 min after injection of ^{64}Cu-ATSM than the SF at 4 and 8 wk after injury (Supplemental Fig. 4), respectively. ^{18}F-FDG imaging demonstrated 2.31 ± 0.29 IF-to-SF SUV_{mean} ratios and 1.82 ± 0.26 IF-to-SF SUV_{max} ratios at 4 and 8 wk after injury (Supplemental Fig. 4). IF-to-BM SUV ratios were significantly higher ($P < 0.001$) than SF-to-BM SUV ratios both 4 and 8 wk after injury after injection of ^{64}Cu-ATSM and 8 wk after injury after injection of ^{18}F-FDG ($P < 0.05$) (Fig. 3).

IF-to-SF SUV ratios measured from ^{64}Cu-ATSM PET images did not show a significant correlation with specific signal on T1-, T2-, or PD-weighted MR images. Nevertheless, the combination of all 3 contrasts helped to delineate the plaque and lumen boundaries. The ratios of IF to SF blood vessel wall cross-sectional areas determined by T1-weighted images was strongly positively correlated to IF-to-SF SUV_{mean} ratios in a linear regression ($R^2 = 0.742$, $P = 0.0002$) (Supplemental Fig. 5). This finding suggested an increasing lipid content and hypoxic level in the IF during the progression of atherosclerosis, as supported by the thickening of the IF blood vessel wall.

Hematoxylin and eosin stain demonstrated a focal thickened neointima composed of foam cells and vascular smooth muscle cells, which was generated in the injured vessel (Supplemental Fig. 6). Immunohistochemical analysis showed that the induced atherosclerotic-like lesions contained macrophages as indicated by RAM-11, which colocalized to the HIF-1α–positive area (Figs. 4A, 4B, and 4D; Supplemental Fig. 7). Hypoxia, as shown by pimonidazole staining of the adjacent section, was located in the deep macrophage-rich area within the atheromatous core of the plaque (Fig. 4C). Superficial macrophages adjacent to the lumen stained negatively with pimonidazole,

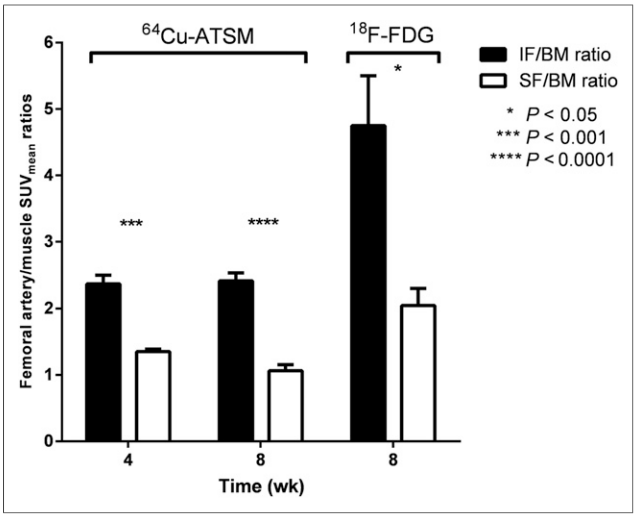

FIGURE 3. IF-to-BM SUV_{mean} ratios were significantly higher than SF-to-BM SUV_{mean} ratios at 4 and 8 wk after injury in ^{64}Cu-ATSM imaging and 8 wk after injury in ^{18}F-FDG imaging.

suggesting that these superficial macrophages were not hypoxic, consistent with what has been described previously (*15*). No immunofluorescence of RAM-11, HIF-1α, or pimonidazole was seen in the sham-operated femoral artery sections (Supplemental Fig. 8).

DISCUSSION

Although ^{64}Cu-ATSM has been investigated for imaging tumor hypoxia in animal and human studies (*16–18*), its use in the assessment of cardiovascular disease has so far been limited. Retrospective review of PET/CT examinations in cervical cancer patients imaged with ^{64}Cu-ATSM at our institution revealed ^{64}Cu-ATSM uptake in regions corresponding to atherosclerosis (personal verbal communication between Farrokh Dehdashti and Pamela K. Woodard). To our knowledge, this study is the first investigation of ^{64}Cu-ATSM as a hypoxic cell PET imaging agent in a nonmurine animal model of atherosclerosis.

Although ^{18}F-FDG, an agent used to image metabolic activity as a glucose analog, has also been used in atherosclerosis imaging (*19*) and has been shown to detect vascular atheroma (*19*), it provides limited value for evaluating the coronary arteries because of the confounding effects of myocardial uptake of the radiotracer. ^{64}Cu-ATSM imaging would overcome this limitation. ^{18}F-fluoromisonidazole is one of the most commonly used investigational PET agents for the measurement of tumor hypoxia (*20*). Recently, the feasibility of this PET imaging agent for in vivo detection of hypoxia in advanced lesions was successfully evaluated in rabbits with advanced atherosclerosis (*15*). However, compared with ^{64}Cu-ATSM, ^{18}F-fluoromisonidazole has 2 major disadvantages: lower cellular uptake and slower washout from normoxic tissue (*20*). The more efficient uptake and washout kinetics of ^{64}Cu-ATSM in hypoxic and normoxic cells offer the possibility of a faster and more selective means of detecting hypoxia by PET imaging. ^{18}F-EF5 has also been studied to detect hypoxic plaques in mice with atherosclerosis by ex vivo methods, but the slow blood clearance and high adventitial uptake limit its value for in vivo imaging of atherosclerosis (*21*). These findings suggest that ^{64}Cu-ATSM has the potential to be a more discriminating agent for hypoxia in atherosclerosis assessment.

Although PET/CT as a hybrid scanner has in the past emerged as a valuable modality in clinical use as well as an important research tool, the fully integrated PET/MR scanners provide the excellent soft-tissue contrast and functional imaging capabilities of MR (*22*). The described morphologic features of plaque vulnerability can be nicely imaged by MRI (*23*), and the biologic features of plaque vulnerability can be visualized by PET with different tracers and targets in a complementary fashion (*24–26*). Thus, PET/MR allows for multiparametric profiling of plaque morphology and potential vulnerability in 1 imaging session and should facilitate the identification of high-risk plaques in patients with atherosclerotic disease (*22*). These nononcologic applications may further benefit from lower radiation exposure of the patients in PET/MR than PET/CT (*27*). In light of these advantages, imaging of atherosclerosis using fully integrated hybrid PET/MR yields an additional diagnostic value both over stand-alone PET and MR scanners and over hybrid PET/CT.

The hematoxylin and eosin stain, along with our previous work (*11*), shows that a combination of a cholesterol-enriched diet and air desiccation produce a focal thickened neointima in the area of air desiccation comprising foam cells and vascular smooth muscle cells. The duration of cholesterol diet in these animals is too short to see lesions induced in peripheral arteries outside the region of air desiccation, thus allowing us to use the contralateral sham artery as a control. The hypoxia-specific dye pimonidazole used for histopathologic characterization ex vivo is a 2-nitroimidazole containing a basic, piperidine moiety and reduces in cells with low oxygen tension. It is

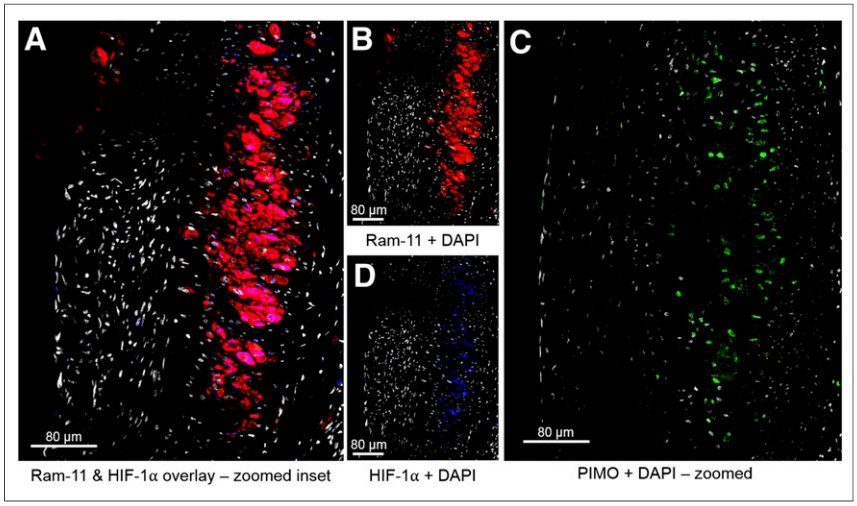

FIGURE 4. In atherosclerotic plaque of injured femoral artery, HIF-1α staining is localized within areas of high RAM-11–positive macrophages (A), confirmed by viewing single-channel staining of RAM-11 (B) and HIF-1α (D). Detection of pimonidazole (PIMO) adducts was done on adjacent slide (C), and pimonidazole positivity was observed in area of RAM-11+HIF-1α displayed in A, B, and D. A and C are at the same scale. For all panels, the color code is as follows: DAPI, white; RAM-11, red; HIF-1α, blue; PIMO, green.

considered the gold standard immunohistochemical hypoxia marker and is widely used as a hypoxia-specific dye ($pO_2 \leq 10$ mm Hg). The resulting pimonidazole derivatives form protein adducts, which can be detected by immunostaining (*28*). This agent has been used primarily in oncologic specimen assessment (*29*) and only recently in assessment of atherosclerosis (*9*). The colocalization of the macrophage marker (RAM-11) and hypoxia indicators (pimonidazole) suggested that the uptake of ^{64}Cu-ATSM was associated with the presence of macrophages. Despite stimuli other than hypoxia that may induce HIF-1 in normoxia (*30*), a previous study (*15*) demonstrated nearly all macrophages present in the plaque expressed HIF-1α, and a strong correlation between the hypoxic region (pimonidazole) and macrophage (RAM-11) density in plaque by immunohistology. Thus, the presence of HIF-1α in the same region as the macrophages in the lesions served as supportive evidence of hypoxia in atherosclerotic macrophages. In addition, the finding that hypoxia was mainly located in the deep, macrophage-rich area within the atheromatous core is consistent with this study (*15*), which suggests that enough oxygen can diffuse from the lumen to nourish the shallow macrophage population but not the deep macrophage-rich core because of the increased consumption or reduced supply of O_2 and nutrients from the lumen and vasa vasorum to those regions. The significantly higher ^{18}F-FDG uptake in the injured femoral artery further helped to confirm the development of advanced plaque and accumulated macrophages in this region. In previous publications, it was shown that macrophages have a high uptake of ^{18}F-FDG (*31*). Moreover, even though we did not assess the biodistribution of ^{64}Cu-ATSM in blood, muscle, and femoral arteries to validate the complete clearance of radiopharmaceuticals at the time periods used for SUV calculation, our methods for SUV comparison—injured femoral–to–sham femoral SUV ratios—show the absence of radioactivity in the blood pool excluding potential bias that could result from the radioactivity contribution from the blood pool (*31*).

One limitation of our study is that the SUVs were not corrected for partial-volume effects (PVEs). The quantitative accuracy of PET is reduced by PVEs primarily because of the limited spatial resolution of the scanner leading to underestimation of the SUV with decreasing structural size of plaques (*32,33*). In practice, PVE is minimal when the dimensions of homogeneous uptake regions are more than 2–3 times the spatial resolution of the scanner (*34*). The spatial resolution of the Siemens mMR PET/MR system is approximately 4.3 mm (*14,35*), whereas the rabbit's femoral artery is 1.5–1.8 mm in diameter (*36*). As a result, quantification of tracer uptake in rabbit atherosclerotic plaque is likely to be significantly affected by PVEs. We are currently developing PVE-correction techniques to exploit the ability of PET/MR to provide high-resolution PET images for improved absolute quantitative assessment of hypoxia in atherosclerotic plaque.

Furthermore, in this project, we used standard multicontrast MRI sequences to image femoral arterial plaque with the initial intent of identifying plaque components in this rabbit model of atherosclerosis. However, because of the relatively small plaque size, limited MRI spatial resolution, and simple plaque components (smooth muscle cells and foam cells), it was difficult to consistently differentiate plaque components by this approach and to obtain quantitative plaque composition information from MR images to conduct specific studies correlating MRI characteristics of atherosclerosis with PET signal.

CONCLUSION

We demonstrated the ability of ^{64}Cu-ATSM PET to noninvasively detect hypoxia in advanced atherosclerosis-like lesions in an animal model. ^{64}Cu-ATSM PET/MR is a promising imaging method for detecting hypoxic and potentially vulnerable atherosclerosis in human subjects.

DISCLOSURE

The costs of publication of this article were defrayed in part by the payment of page charges. Therefore, and solely to indicate this fact, this article is hereby marked "advertisement" in accordance with 18 USC section 1734. This work was supported by a pilot grant from the Diabetic Cardiovascular Disease Center (DCDC), Washington University School of Medicine, the Washington University Institute of Clinical and Translational Sciences grant UL1TR000448 from the National Center for Advancing Translational Sciences (NCATS) of the National Institutes of Health (NIH), Department of Energy grant DESC0002032, and NIH National Research Service Award (5-T32-HL07081-38) from the National Heart, Lung and Blood Institute. No other potential conflict of interest relevant to this article was reported.

ACKNOWLEDGMENTS

We thank Nicole Fettig, Margaret Morris, Amanda Roth, Lori Strong, Ann Stroncek, Glenn Foster, Linda Becker, Michael Harrod, Pamela Baum, and David Muccigrosso for their assistance with the imaging studies; Susie Grathwohl and Rich Pierce for their technical help with animal surgery and postoperative monitoring; and the isotope production team at Washington University for ^{64}Cu production.

REFERENCES

1. Virmani R, Kolodgie FD, Burke AP, Farb A, Schwartz SM. Lessons from sudden coronary death: a comprehensive morphological classification scheme for atherosclerotic lesions. *Arterioscler Thromb Vasc Biol.* 2000;20:1262–1275.
2. Lusis AJ. Atherosclerosis. *Nature.* 2000;407:233–241.
3. Hansson GK. Inflammation, atherosclerosis, and coronary artery disease. *N Engl J Med.* 2005;352:1685–1695.
4. Hueper WC. Arteriosclerosis. *Arch of Pathol.* 1944;38:0350–0364.
5. Libby P, DiCarli M, Weissleder R. The vascular biology of atherosclerosis and imaging targets. *J Nucl Med.* 2010;51(suppl 1):33S–37S.
6. Leppänen O, Bjornheden T, Evaldsson M, Boren J, Wiklund O, Levin M. ATP depletion in macrophages in the core of advanced rabbit atherosclerotic plaques in vivo. *Atherosclerosis.* 2006;188:323–330.
7. Hultén LM, Levin M. The role of hypoxia in atherosclerosis. *Curr Opin Lipidol.* 2009;20:409–414.
8. Björnheden T, Levin M, Evaldsson M, Wiklund O. Evidence of hypoxic areas within the arterial wall in vivo. *Arterioscler Thromb Vasc Biol.* 1999; 19:870–876.
9. Sluimer JC, Gasc JM, van Wanroij JL, et al. Hypoxia, hypoxia-inducible transcription factor, and macrophages in human atherosclerotic plaques are correlated with intraplaque angiogenesis. *J Am Coll Cardiol.* 2008;51:1258–1265.
10. Zheng J, Ochoa E, Misselwitz B, et al. Targeted contrast agent helps to monitor advanced plaque during progression: a magnetic resonance imaging study in rabbits. *Invest Radiol.* 2008;43:49–55.
11. Liu Y, Abendschein D, Woodard GE, et al. Molecular imaging of atherosclerotic plaque with ^{64}Cu-labeled natriuretic peptide and PET. *J Nucl Med.* 2010;51:85–91.
12. Kume M, Carey PC, Gaehle G, et al. A semi-automated system for the routine production of copper-64. *Appl Radiat Isot.* 2012;70:1803–1806.
13. Voller TF. Procedure: preparation of ^{64}Cu-diacetyl-bi [N4-methylthiosemicarbazone] (^{64}Cu-ATSM). St. Louis, MO: Washington University School of Medicine; 2008.
14. Delso G, Furst S, Jakoby B, et al. Performance measurements of the Siemens mMR integrated whole-body PET/MR scanner. *J Nucl Med.* 2011;52:1914–1922.
15. Mateo J, Izquierdo-Garcia D, Badimon JJ, Fayad ZA, Fuster V. Noninvasive assessment of hypoxia in rabbit advanced atherosclerosis using ^{18}F-fluoromisonidazole positron emission tomographic imaging. *Circ Cardiovasc Imaging.* 2014;7: 312–320.

16. Lewis JS, McCarthy DW, McCarthy TJ, Fujibayashi Y, Welch MJ. Evaluation of ^{64}Cu-ATSM in vitro and in vivo in a hypoxic tumor model. *J Nucl Med.* 1999; 40:177–183.
17. Lewis JS, Sharp TL, Laforest R, Fujibayashi Y, Welch MJ. Tumor uptake of copper-diacetyl-bis(N(4)-methylthiosemicarbazone): effect of changes in tissue oxygenation. *J Nucl Med.* 2001;42:655–661.
18. Dehdashti F, Grigsby PW, Mintun MA, Lewis JS, Siegel BA, Welch MJ. Assessing tumor hypoxia in cervical cancer by positron emission tomography with ^{60}Cu-ATSM: relationship to therapeutic response-a preliminary report. *Int J Radiat Oncol Biol Phys.* 2003;55:1233–1238.
19. Rudd JH, Myers KS, Bansilal S, et al. ^{18}Fluorodeoxyglucose positron emission tomography imaging of atherosclerotic plaque inflammation is highly reproducible: implications for atherosclerosis therapy trials. *J Am Coll Cardiol.* 2007;50:892–896.
20. Bourgeois M, Rajerison H, Guerard F, et al. Contribution of [^{64}Cu]-ATSM PET in molecular imaging of tumour hypoxia compared to classical [^{18}F]-MISO: a selected review. *Nucl Med Rev Cent East Eur.* 2011;14:90–95.
21. Silvola JM, Saraste A, Forsback S, et al. Detection of hypoxia by [^{18}F]EF5 in atherosclerotic plaques in mice. *Arterioscler Thromb Vasc Biol*. 2011; 31:1011–1015.
22. Rischpler C, Nekolla SG, Beer AJ. PET/MR imaging of atherosclerosis: initial experience and outlook. *Am J Nucl Med Mol Imaging.* 2013;3:393–396.
23. Saam T, Hatsukami TS, Takaya N, et al. The vulnerable, or high-risk, atherosclerotic plaque: noninvasive MR imaging for characterization and assessment. *Radiology.* 2007;244:64–77.
24. Rudd JH, Warburton EA, Fryer TD, et al. Imaging atherosclerotic plaque inflammation with [^{18}F]-fluorodeoxyglucose positron emission tomography. *Circulation.* 2002;105:2708–2711.
25. Temma T, Saji H. Radiolabelled probes for imaging of atherosclerotic plaques. *Am J Nucl Med Mol Imaging.* 2012;2:432–447.
26. Nolting DD, Nickels ML, Guo N, Pham W. Molecular imaging probe development: a chemistry perspective. *Am J Nucl Med Mol Imaging.* 2012;2:273–306.
27. Balyasnikova S, Lofgren J, de Nijs R, Zamogilnaya Y, Hojgaard L, Fischer BM. PET/MR in oncology: an introduction with focus on MR and future perspectives for hybrid imaging. *Am J Nucl Med Mol Imaging.* 2012;2:458–474.
28. Mayr M, Sidibe A, Zampetaki A. The paradox of hypoxic and oxidative stress in atherosclerosis. *J Am Coll Cardiol.* 2008;51:1266–1267.
29. Janssens GO, Rademakers SE, Terhaard CH, et al. Accelerated radiotherapy with carbogen and nicotinamide for laryngeal cancer: results of a phase III randomized trial. *J Clin Oncol.* 2012;30:1777–1783.
30. Dehne N, Brune B. HIF-1 in the inflammatory microenvironment. *Exp Cell Res.* 2009;315:1791–1797.
31. Zhang Z, Machac J, Helft G, et al. Non-invasive imaging of atherosclerotic plaque macrophage in a rabbit model with F-18 FDG PET: a histopathological correlation. *BMC Nucl Med.* 2006;6:3.
32. Mazziotta JC, Phelps ME, Plummer D, Kuhl DE. Quantitation in positron emission computed tomography: 5. Physical–anatomical effects. *J Comput Assist Tomogr.* 1981;5:734–743.
33. Izquierdo-Garcia D, Davies JR, Graves MJ, et al. Comparison of methods for magnetic resonance-guided [18-F]fluorodeoxyglucose positron emission tomography in human carotid arteries: reproducibility, partial volume correction, and correlation between methods. *Stroke.* 2009;40:86–93.
34. Hoffman EJ, Huang SC, Phelps ME. Quantitation in positron emission computed tomography: 1. Effect of object size. *J Comput Assist Tomogr.* 1979;3:299–308.
35. Biograph mMR: technical details. Siemens Healthcare GmbH website. http://www.healthcare.siemens.com/magnetic-resonance-imaging/mr-pet-scanner/biograph-mmr/technical-details. Accessed August 24, 2016.
36. Wang W, Chang T-S, Sun Y-L. Chapter 3: basic techniques and operative methods in microsurgery. In: Chang T-S, ed. *Principles, Techniques and Applications in Microsurgery.* Singapore: World Scientific Publishing Company; 1986: 30.